Experimental and Numerical Investigations of an Inflated Air-Spring Made of Fiber-Reinforced Rubber

Asst. Prof. Dr. Mohsin Noori Hamzah
Mechanical Engineering Department,
University of Technology
Email: dr.mohsin@uotechnology.edu.iq

Mahmood Shakir Nima
(M.Sc. student)
Mechanical Engineering Department
University of Technology
Email: darknewton89@yahoo.com

Received 13 April 2015 Accepted 9 June 2015

ABSTRACT

Air-springs are characterized by strongly anisotropic material behavior and can simultaneously undergo large elastic deformations. This attribute involves an appropriate constitutive model for an adequate numerical simulation of these components' complex response. The present paper discusses the manufacturing process of an air-spring and deals with the use of anisotropic-based hyperelastic constitutive model in the context of thin membranes inflation. In order to investigate the capability of the proposed model, some finite element analysis were conducted by using ANSYS 15.0. The proposed model shows a good predictive ability and exhibits a good agreement when compared to the experimental work of the present paper.

NOMENCLATURES

C	Right Cauchy deformation tensor
F	Deformation gradient tensor
I_1, I_2	Strain invariants
I_4, I_6	Pseudo strain invarients
J	Volume ratio
S	2nd Piola-Kirchhof stress N/m^2
NR	Natural Rubber

Keywords: air-spring, fiber-reinforced rubber composite, hyperelastic constitutive modeling, anisotropy, finite element analysis.

دراسة عملية ونظرية لنابض هوائي مصنوع من مطاط مدعم بالألياف

أ. م. د. محسن نوري حمزة
Email: dr.mohsin@uotechnology.edu.iq

محمود شاكر نعمة
Email: darknewton89@yahoo.com

الخلاصة:

تتمتع النوابض الهوائية بخصائص اتجاهية وتمتاز بقابليتها على تحمل تشوهات عالية. هذه الميزات تتطلب إيجاد نموذج صالح لوصف تصرف هذه الأجزاء الميكانيكية. هذا البحث يهتم بدراسة طريقة تصنيع النوابض الهوائية، واشتقاق نموذج لوصف تصرف المرونة الشديدة فيها. تم اجراء تحليلات عددية باستخدام برنامج (ANSYS 15.0)، لغرض التحقق من صحة النوذج المقترح والذي أظهر توافق جيد وبصورة مرضية عند مقانة النتائج النظرية مع النتائج العملية للبحث.

1. INTRODUCTION

The inflation of hyperelastic rubber-like membranes has been extensively studied in the past. There are two different approaches used to solve this type of problems: the first approach is based on the analytical solutions, while the second one is based on the application of the finite element method (FEM) to the problems of membrane inflation.

In the context of the first approach, the governing equations of the large strains inflation of axisymmetric membranes were established by **(Green and Adkins, 1960)**. Following the same approach, authors, e.g., **(Guo, 2001), (Kydoniefs and Spencer, 1969)**, **(Yang and Feng, 1970)** and **(Khayat et al., 1992)** attempted to solve the problem of the inflation of membranes from an analytical perspective. **(Guo, 2001)** studied the large deformation of a cylindrical hyperelastic membrane circumferentially bonded and sealed at each end to a rigid tube. **(Kydoniefs and Spencer, 1969)** obtained an exact general solution of the equations of finite deformations of elastic membranes and applied it to the problem of inflation of a cylinder of finite length sealed at each end by rigid plugs. **(Yang and Feng, 1970)** reformulated the mechanics problem concerning large axisymmetric deformations of nonlinear membranes in terms of a system of three first-order ordinary differential equations with explicit derivatives. Moreover, **(Khayat et al., 1992)** detailed the occurrence of unstable behaviors in the inflation of Neo-Hookean membranes with non-uniform radius and thickness.

In the context of the finite element method, a simple finite element formulation was presented by **(Jiang and Haddow, 1995)** for finite static axisymmetric deformation of isotropic incompressible hyperelastic membranes. That finite element procedure was derived from a finite deformation membrane theory, in which Lagrangian type equilibrium equations, expressed in terms of the Biot stresses were employed along with constitutive equations relating the principal components of the Biot stress tensor and of the principal stretches. Based on Ogden's non-linear elastic material law, an axisymmetrical membrane element for large deformations was developed by **(Wriggers and Taylor, 1990)**. More recently, **(Shi and Moita, 1996)** studied post-critical response in the inflation of axisymmetric membranes. They performed an extensive parametric study to investigate the non-linear response of a tube under internal pressure. **(Verron and Marckmann, 2001)** presented an axisymmetric B-spline model for the non-linear inflation of both cylindrical and spherical Mooney-Rivlin membranes. Later on, a finite element method was presented by **(Kyriacou et al., 1996)** for geometrically and materially nonlinear orthotropic hyperelastic membranes. The constitutive relations were formulated in terms of the invariants of the 2D right Cauchy-Green strain tensor and the resulting system of nonlinear equations was solved using a Newton-Raphson approach. **(Resse et al., 2001)** developed a model to describe the hypereleastic material behavior of pneumatic membrane reinforced with roven-woven fibers. The numerical simulation of a cylindrical membrane was developed for anisotropic hyperelastic materials by **(Marvalová and Nam, 2003)**. Recently, **(Abdessalem et al., 2011)** described a general finite element implementation framework for the constitutive modeling of biological soft tissues.

The aim of the present paper is to manufacture an inflated air-spring membrane and propose an anisotropic-based hyperelastic constitutive model that predicts the complex behavior of the membrane. Moreover, performing some finite element analyses is another goal of this paper, in

order to compare the theoretical response of the membrane with the experimental one and check the validity of the model in solving such a type of problems.

2. EXPERIMENTAL WORK

2.1 The Fabrication of the Air-Spring

Typically, an air-spring consists of two basic components; a flexible member (the rubbery component) and fixation parts (metal components). The first step of the experimental procedure in this part was to make a mold for manufacturing the flexible member of the air spring according to the desired dimensions. The mold, as shown in **Figure 1**, was manufactured from steel and consisted of two major parts; the drum, and the top cover. The cavity of the mold is situated between the drum and the top cover.

The manufacturing steps used for manufacturing the air-spring are briefly summarized in the following steps:

- The rubber blend recipe, shown in **Table 1**, was mixed together by using a 2-roll calendering machine according to the rules followed in such processes until reaching complete homogenous blend. The rubber liner produced from calendaring process was coated with a chemical solution prepared by dissolving pieces of the same rubber blend into Heptane to enhance the adhesion between the layer of fibers and the rubber liner, as shown in **Figure 2-a**.
- A layer of Polyester fibers was oriented in 45° with respect to the vertical direction above the rubber liner (**Figure 2-b**), and again the chemical solution was added to the fibers, **Figure 2-c**.
- Another liner of rubber blend was placed above the layer of fibers forming the first ply of fiber-reinforced rubber composite, **Figure 2-d**.
- Another ply of fiber-reinforced rubber composite was fabricated in the same manner and placed on the first one in such a way that the layers of fibers were perpendicular to each other, i.e. the layers of fibers were [45/-45] with respect to the vertical.
- The mold was coated with a demoulding spray in order to facilitate the demounting of the flexible member of the air-spring out of the mold after curing process.
- The two fabricated uncured plies of fiber-reinforced rubber composite were then applied to the building drum of the mold as shown in **Figure 2-e**. The excessive parts of the uncured plies were removed, **Figure 2-f**.
- Heat and pressure were applied to effect vulcanization of the spring as shown in **Figure 2-g**. The cured flexible member was then removed from the mold and inspected, **Figure 2-h**.
- The metal components and the fixation parts for the flexible member were designed and manufactured and then assembled together with the flexible member, **Figure 2-i**, in such a way that the lower end of the air spring is fixed and the upper one is moveable. The air is to be supplied from the lower end via a one-way valve.

2.2 Samples Preparation and Tensile Tests

The samples preparing processes and tests were done in Babylon Tire Factory laboratories. One of the manufactured flexible members, shown in **Figure 2-h**, was used to harvest the fiber-rubber composite dumbbell specimens. These specimens were cut in each direction of each layer of fibers as shown in **Figure 3**.

This test was carried out by using Monsanto Tensometor 10. The effective length of the sample is the distance between the two holders, which was fixed at length (25 mm) according to the ASTM D412. The composite specimens were tested under a quasi-static speed. The mechanical response of the specimens is shown in **Figure. 4**.

2.3 The Test Rig

In order to check the validity of the proposed model, the air-spring was manufactured in order to be used in a test rig. Generally, air-springs are used for actuation and isolation tasks within industrial equipment and within vehicle suspensions. They can replace the metal springs resulting in lighter vehicles and softer riding.

The loading for the test rig was meant to mimic the working conditions for an air-spring. Firstly, the manufactured air-spring was gradually subjected to internal pressure of 0.1 MPa via the valve on the fixed lower end of the air-spring. This test was carried out by using the tensile test instrument by which an axial displacement was exerted on the moveable upper end of the air-spring. The pressurized air-spring was placed between the jaws of the tensile test instrument. The experimental tests were carried out at four different positions of the air-spring. Before each stage of loading the inner pressure of the air-spring was measured by using a dial gauge in order to make sure that the pressure was still at the desired value. The mounting plates of the air-spring were at the free height position of the air-spring and then the upper jaw of the tensile test instrument was given a downward movement at a very low speed to fix the upper end of the air-spring at the distance of 5, 10 and 15 mm shorter than the free height.

A high-definition digital camera was fixed on a fixed tripod in such a way that the plane of the lens of the camera was facing the air-spring and was perpendicular to the ground as depicted in **Figure 5**. For each case, the inflation profile was captured by the fixed digital camera as shown in **Figure 6**. The captured images were fed to Plot Digitizer ver. 1.9 to track the deformed side profile of the air-spring. The images were calibrated via three non-collinear points of which the Cartesian coordinates are known, then by clicking multiple points on the path of interest, a table of data representing the deformed side profile of the air-spring was created. That table was exported to MS Excel and the corresponding deformation of the inflated air-spring was calculated and plotted as shown in **Figure 7**, in order to be compared later with that to be obtained from ANSYS.

3. Constitutive Modeling

The composite elastomers is considered as an anisotropic hyperelastic and continuous solid, which can be described by the coordinates system X in undeformed state. After deformation the body may be described by the coordinate system x. The deformation gradient, **F**, defined as $\mathbf{F} = \partial \mathbf{x} / \partial \mathbf{X}$, and the volume ratio, *J*, expressed as $J = |\mathbf{F}| > 0$.

The deformation gradient can be decomposed into volumetric and distortional deformation, $\mathbf{F} = \left(J^{1/3}\right)\bar{\mathbf{F}}$. Similarly, for the right Cauchy-Green tensor

$$\mathbf{C} = \mathbf{F}^{\mathrm{T}}\mathbf{F} = \left(J^{2/3}\right)\bar{\mathbf{C}}, \qquad \bar{\mathbf{C}} = \bar{\mathbf{F}}^{\mathrm{T}}\bar{\mathbf{F}} \tag{1}$$

The Helmholtz free energy can be decoupled into the volumetric and isochoric parts. Furthermore, the isochoric part can be divided into an isotropic (independent of fiber orientations) and an anisotropic part:

$$\Psi = \Psi_{\text{vol}}(J) + \Psi_{\text{iso}}(\bar{\mathrm{C}}) + \Psi_{\text{aniso}}(\bar{\mathbf{C}}, \mathbf{a}\otimes\mathbf{a}, \mathbf{g}\otimes\mathbf{g}) \quad (2)$$

where **a** and **g** are two fiber directions in the undeformed configuration, **Figure 8**, characterizing the anisotropic behavior of the material, and $|\mathbf{a}| = 1,$ and $|\mathbf{g}| = 1$.

The isochoric part of the strain energy functions can be written in terms of strain invariants, the isotropic part in terms of $\bar{I}_1$. Additionally, the anisotropic part was written in terms of pseudo-invariants, $\bar{I}_4$ and $\bar{I}_6$ only, since they are the squares of the stretches in the directions of the fibers, and therefore have a physical interpretation **(Holzapfel et al., 2000)**. The strain energy in terms of the modified invariants will be:

$$\Psi = \Psi_{vol}(J) + \Psi_{iso}(\bar{I}_1) + \Psi_{aniso}(\bar{I}_4, \bar{I}_6) \quad (3)$$

where $\bar{I}_1 = tr\ \bar{\mathbf{C}}$, $\bar{I}_4 = \mathbf{a}\cdot\bar{\mathbf{C}}\mathbf{a}$, and $\bar{I}_6 = \mathbf{g}\cdot\bar{\mathbf{C}}\mathbf{g}$.

The volumetric part of the strain energy function is given by:

$$\Psi_v(J) = \frac{1}{d}(J-1)^2 \quad (4)$$

The isotropic part of the strain energy function used in this paper is the two term Yeoh model **(Yeoh, 1993):**

$$\Psi_{iso}(\bar{I}_1) = B_{10}(\bar{I}_1 - 3) + B_{20}(\bar{I}_1 - 3)^2 \quad (5)$$

While the anisotropic part of the strain energy function; i.e. the energy function in the fibers, is assumed in the form of an exponential form **(Holzapfel, 2000, Hamzah, 2013):**

$$\Psi_{aniso}(\bar{I}_4, \bar{I}_6) = \frac{c_1}{2c_2}[\exp(c_2(\bar{I}_4 - 1)^2 - 1)] + \frac{e_1}{2e_2}[\exp(e_2(\bar{I}_6 - 1)^2 - 1)] \quad (6)$$

where c_1 and e_1 are stress-like material parameters and c_2 and e_2 are dimensionless parameters **(Holzapfel, 2000).**

In order to determine the constitutive equations for anisotropic hyperelastic materials in term of strain invariants, the strain energy function, Ψ, is differentiated with respect to tensor **C**. By means of the chain rule, the second Piola-Kirchhoff stress (2nd PK), $\boldsymbol{\mathcal{S}}$, can be obtained by decomposing it into volumetric and the deviatoric stress :

$$\boldsymbol{\mathcal{S}} = \boldsymbol{\mathcal{S}}_{\boldsymbol{vol}} + \boldsymbol{\mathcal{S}}_{\boldsymbol{iso}} + \boldsymbol{\mathcal{S}}_{\boldsymbol{ani}} = \boldsymbol{\mathcal{S}}_{\boldsymbol{vol}} + \boldsymbol{\mathcal{S}}_{\boldsymbol{div}} \quad (7)$$

Where $\boldsymbol{\mathcal{S}}_{\boldsymbol{vol}}$ and $\boldsymbol{\mathcal{S}}_{\boldsymbol{div}}$ are the volumetric and the deviatoric stress, which they can be expressed as:

$$\mathcal{S}_{\text{vol}} = p\,J\,\mathrm{C}^{-1}, \quad (8)$$

$$\boldsymbol{\mathcal{S}}_{\boldsymbol{div}} = J^{-2/3}\left(\bar{\boldsymbol{\mathcal{S}}} - \frac{1}{3}\left(\bar{\mathbf{C}}:\bar{\boldsymbol{\mathcal{S}}}\right)\bar{\mathbf{C}}^{-1}\right) \quad (9)$$

and,

$$\widetilde{\boldsymbol{S}} = 2\frac{\partial \Psi_{div}}{\partial \bar{\mathbf{C}}} = 2\sum_{\alpha=1,2,4,6}^{4} \frac{\partial \Psi_{div}}{\partial \bar{I}_{\alpha}} \frac{\partial \bar{I}_{\alpha}}{\partial \bar{\mathbf{C}}} \tag{10}$$

The derivatives of the modified invariants with respect to the deviatoric part of the right Cauchy-Green tensor are written as:

$$\frac{\partial \bar{I}_1}{\partial \bar{\mathbf{C}}} = \mathbf{I},\ \frac{\partial \bar{I}_4}{\partial \bar{\mathbf{C}}} = \mathbf{a}\otimes\mathbf{a},\ \text{and}\ \frac{\partial \bar{I}_6}{\partial \bar{\mathbf{C}}} = \mathbf{g}\otimes\mathbf{g} \tag{11a}$$

The derivatives of the deviatoric part of the strain energy function with respect to the deviatoric part of the strain invariants;

$$\begin{aligned} \frac{\partial \Psi_{div}}{\partial \bar{I}_1} &= B_{10} + 2\ B_{20}\,(\bar{I}_1 - 3) \\ \frac{\partial \Psi_{div}}{\partial \bar{I}_4} &= c_1(\bar{I}_4 - 1)\exp(c_2(\bar{I}_4 - 1)^2) \\ \frac{\partial \Psi_{div}}{\partial \bar{I}_6} &= e_1(\bar{I}_6 - 1)\exp(e_2(\bar{I}_6 - 1)^2) \end{aligned} \tag{11b}$$

The Cauchy (true) stress can be computed from the 2nd PK as,

$$\boldsymbol{\sigma} = J^{-1}\mathbf{F}\boldsymbol{S}\mathbf{F}^{T} \tag{12}$$

For uniaxial tension, assuming full incompressibility, i.e., J=1, $\lambda_1 = \lambda$ and, $\lambda_2 = \lambda_3 = \lambda^{-1/2}$, therefore

$$\mathbf{F} = \begin{bmatrix} \lambda & 0 & 0 \\ 0 & \lambda^{-1/2} & 0 \\ 0 & 0 & \lambda^{-1/2} \end{bmatrix}$$

The derivatives of the modified invariants will be,

$$\frac{\partial \bar{I}_1}{\partial \bar{\mathbf{C}}} = \mathbf{I}$$

$$\frac{\partial \bar{I}_4}{\partial \bar{\mathbf{C}}} = \begin{bmatrix} \cos^2(\beta_1) & \sin(\beta_1)\cos(\beta_1) & 0 \\ \sin(\beta_1)\cos(\beta_1) & \sin^2(\beta_1) & 0 \\ 0 & 0 & 0 \end{bmatrix}$$

$$\text{and}\ \frac{\partial \bar{I}_6}{\partial \bar{\mathbf{C}}} = \begin{bmatrix} \cos^2(\beta_2) & \sin(\beta_2)\cos(\beta_2) & 0 \\ \sin(\beta_2)\cos(\beta_2) & \sin^2(\beta_2) & 0 \\ 0 & 0 & 0 \end{bmatrix}$$

where β_1 and β_2 are the angles of the first layer and the second layer of fibers, respectively, measured in counterclockwise direction from 1-axis, **Figure 8**.

Using the above equations with equation (7) obtain:

$$\begin{bmatrix} S_{11} & S_{12} & S_{13} \\ S_{21} & S_{22} & S_{23} \\ S_{31} & S_{32} & S_{33} \end{bmatrix} = p \begin{bmatrix} \lambda^{-2} & 0 & 0 \\ 0 & \lambda & 0 \\ 0 & 0 & \lambda \end{bmatrix} + \begin{bmatrix} \tilde{S}_{11} & \tilde{S}_{12} & \tilde{S}_{13} \\ \tilde{S}_{21} & \tilde{S}_{22} & \tilde{S}_{23} \\ \tilde{S}_{31} & \tilde{S}_{32} & \tilde{S}_{33} \end{bmatrix} - \frac{\lambda^2 \tilde{S}_{11} + \lambda^{-1}(\tilde{S}_{22} + \tilde{S}_{33})}{3} \begin{bmatrix} \lambda^{-2} & 0 & 0 \\ 0 & \lambda & 0 \\ 0 & 0 & \lambda \end{bmatrix} \quad (13)$$

Since the stresses in the 2 and 3-axes are zero in the case of the uniaxial test, therefore an expression for the hydrostatic pressure can be obtained from equation (13), then substituting the obtained expression of the hydrostatic pressure for the stress S_{11} in 1-axis, this yields the following constitutive relation,

$$S_{11} = \tilde{S}_{11} - \frac{\tilde{S}_{33}}{\lambda^3} \quad (14)$$

where

$$\tilde{S}_{11} = 2\,B_{10} + 4\,B_{20}\,(\bar{I}_1 - 3) + 2[c_1(\bar{I}_4 - 1)\exp(c_2(\bar{I}_4 - 1)^2)]\cos^2(\beta_1) +$$
$$2[e_1(\bar{I}_6 - 1)\exp(e_2(\bar{I}_6 - 1)^2)]\cos^2(\beta_2)$$
$$\tilde{S}_{33} = 2\,B_{10} + 4\,B_{20}\,(\bar{I}_1 - 3)$$

The material parameters identification was achieved by means of non-linear least-square and a Levenberg-Marquardt type algorithm to find the best fit for the proposed model, **Figure 9**. All of the obtained material parameters are shown in **Table 2**.

4. Finite Element Analysis

The simulation of deformation was implemented in the finite element method, using ANSYS 15.0. After creating the geometry of the flexible member of the air-spring, the model was meshed with element type SOLID186 which supports hyperelasticity. The direction of the layers of fibers of [45/-45] with respect to the vertical direction and the material parameters of the proposed model were fed into ANSYS via AHYPER command, this APDL (ANSYS Parametric Design Language) command is used to solve the problems of anisotropic hyperelasticity materials. The command receives the material parameters table through TB command for volumetric part, the isochoric part and the material directions.

The boundary conditions were applied as follows: the lower end of the model was fixed, while the upper one was fixed at its free height position. A pressure of 0.1 MPa was applied to the inner surface of the model. All the previous steps were repeated for axial displacements of 5, 10 and 15 mm.

For each state of loading, a path on the line in interest was defined by choosing multiple nodes on the side profile of the deformed shape of the model. This path was mapped onto the amount of deformation in the radial direction. The data resulted from that procedure were fed to MS Excel and compared to that obtained in the experimental test rig for each stage of loading as shown in **Figure. 7**.

Being concerned with the maximum deformation, as one of the criteria for designing the flexible member of the air-spring, the maximum value of predicted deformations are compared to that obtained from the experimental test rig for each stage of loading. **Table 3** summarizes the accuracy achieved by the proposed model by using the following equation:

$$Percentage\ Error = \frac{experimental\ value - predicted\ value}{predicted\ value} * 100 \quad (15)$$

5. Conclusions

- The proposed anisotropic hyperelastic constitutive model was based on the decomposition of the strain energy function into isotropic and anisotropic components. The isotropic component was described by a polynomial form of strain energy (Yeoh model) with two material parameters. While, an exponential form of the strain energy function with two material parameters for each layer of fibers were used for the anisotropic component.
- The discrepancies between test data and simulated data might not vanish completely, which are due to, the fact that the mathematical model cannot completely describe the mechanical behavior of the material, probable imperfections during the manufacturing process and uncertainties in laboratory tests.
- The proposed hyperelastic model gave a very good agreement with the experimental results with relatively low number of material parameters to be determined from only a uniaxial extension.

References

[1] Abdessalem J., Kallel I.K., Fakhreddine D., "Theory and finite element implementation of orthotropic and transversely isotropic incompressible hyperelastic membrane", *Multidiscipline Modeling in Materials and Structures* Vol. 7, No. 4, pp. 424-439, 2011.

[2] Green A.E., Adkins J.E., *Large elastic deformations and non-linear continuum mechanics*, Clarendon Press, Oxford, 1960.

[3] Guo X., "Large deformation analysis for a cylindrical hyperelastic membrane of rubber-like material under internal pressure", *Rubber Chemistry and Technology*, Vol. 74, No. 1, pp. 100-115, 2001.

[4] Hamzah M.N., Subit D, Boruah S., Forman J., Crandall J., Ito D., Ejima S., Kamiji K., Yasuki T., "An inverse finite element approach for estimating the fiber orientations in intercostal muscles", *IRCOBI Conference 2013*, Gothenburg, pp. 722-733, 2013.

[5] Holzapfel G.A., Gasser T.C., Ogden R.W., "A new constitutive framework for arterial wall mechanics and a comparative study of material models", *Journal of Elasticity*, Vol. 61, pp. 1-48, 2000.

[6] Jiang L., Haddow J.B., "A finite element formulation for finite static axisymmetric deformation of hyperelastic membranes", *Computers and Structures*, Vol. 57, No. 3, pp. 401-405, 1995.

[7] Khayat R. E., Derdouri A., Garcia-Rejon A., "Inflation of an elastic cylindrical membrane: non-linear deformation and instability", *International Journal of Solids and Structures*, Vol. 29, No. 1, pp. 69-87, 1992.

[8] Kydoniefs A.D., Spencer A.J.M., "Finite axisymmetric deformations of an initially cylindrical elastic membrane", *Quarterly Journal of Mechanics and Applied Mathematics*, Vol. 22, No. 1, pp. 87-95, 1969.

[9] Kyriacou S. K., Humphrey J. D., Schwab C., "Finite element analysis of nonlinear orthotropic hyperelastic membranes", *Computational Mechanics*, Vol. 18, No. 4, pp. 269-278, 1996.

[10] Marvalová B., Nam T.H., "Deformation analysis of an inflated cylindrical membrane of composite with rubber matrix reinforced by textile material cords", *Proceedings of the International Conference on Engineering Mechanics*, Svratka, Czech Republic, pp. 194-195, 2003.

[11] Reese S., Raible T., Wriggers P., "Finite element modeling of orthotropic material behavior in pneumatic membranes", *International Journal of Solids and Structures*, Vol. 38, pp. 9525-9544, 2001.

[12] Shi J., Moita G.F., "The post-critical analysis of axisymmetric hyperelastic membranes by finite element method", *Computer Methods in Applied Mechanics and Engineering*, Vol. 135, pp. 265-281, 1996.

[13] Verron E., Marckmann G., "An axisymmetric B-spline model for the non-linear inflation of rubber-like membranes", *Computer Methods in Applied Mechanics and Engineering*, Vol. 190, pp. 6271- 6289, 2001.

[14] Wriggers P., Taylor R.L., "A fully non-linear axisymmetrical membrane element for rubber-like materials", *Engineering Computations*, Vol. 7, No. 4, pp. 303-310, 1990.

[15] Yang W.H., Feng W.W., "On axisymmetrical deformations of nonlinear membranes", *Journal of Applied Mechanics*, Vol. 37, No. 4, pp. 1002-1011, 1970.

[16] Yeoh O.H., "Some forms of the strain energy function for Rubber", *Rubber Chemistry and Technology*, Vol. 66, Issue 5, pp. 54-771, 1993.

Table (1): The rubber blend recipe.

Material	PHR
NR	100
Renacit	0.1
Zinc Oxide	5
Stearic Acid	1.9
Carbon N326	46.5
Process oil	6.89
Phenol tack resin	0.55
Recorcinol	1.59
TMQ	1.1
MBS	0.53
CTP-100	0.21
HMT	0.84
Insoluble Sulphur	3.39

Table (2): Material parameters obtained from curve fitting process.

B_{10}(MPa)	B_{20}(MPa)	c_1(MPa)	c_2	e_1(MPa)	e_2
1.653	-0.3287	63.33	-0.06319	63.33	-0.06319

Table (3): Comparison of maximum deformation between the experimental test rig and FEA analysis.

	At free height	Displacements		
		5 mm	10 mm	15 mm
experimental deformation	3.131	4.688	7.035	9.279
predicted deformation	3.444	5.104	7.448	9.695
Error %	9.088	8.15	5.545	4.291

(*a*) (*b*)

Figure (1): The manufactured mold, (a) the drum, (b) the top cover.

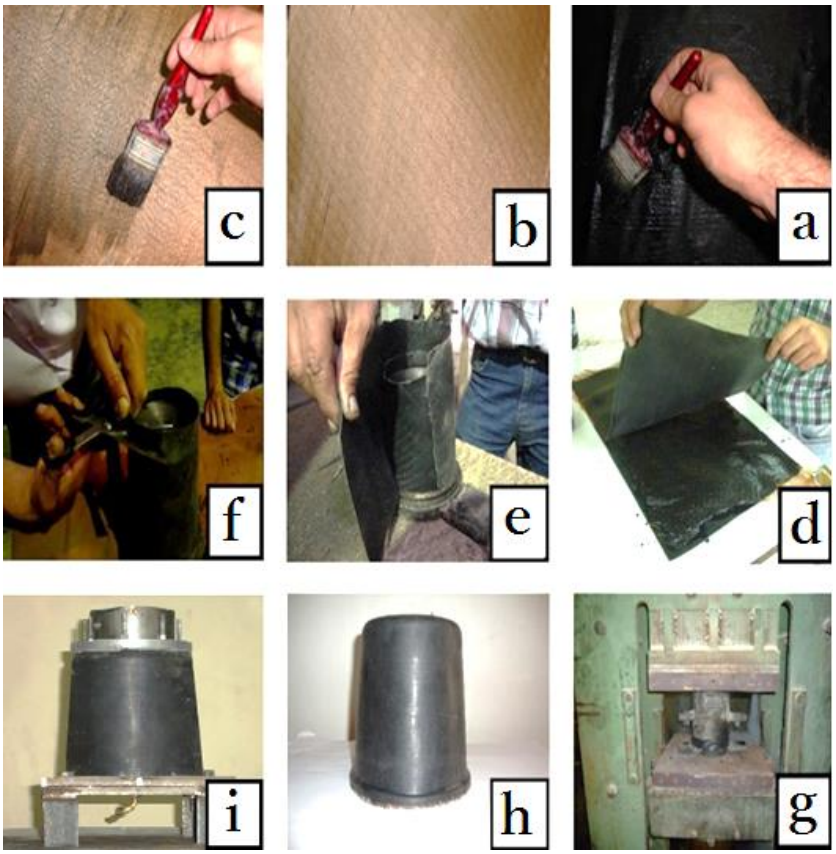

Figure (2): Manufacturing steps of the air spring.

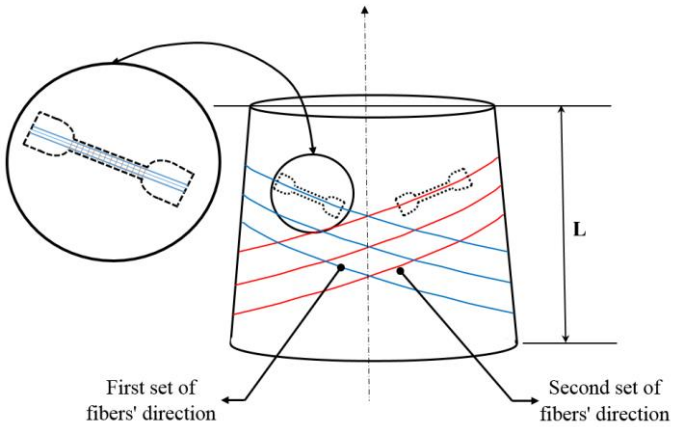

Figure (3): The fiber-rubber specimens cut in each fibers' direction.

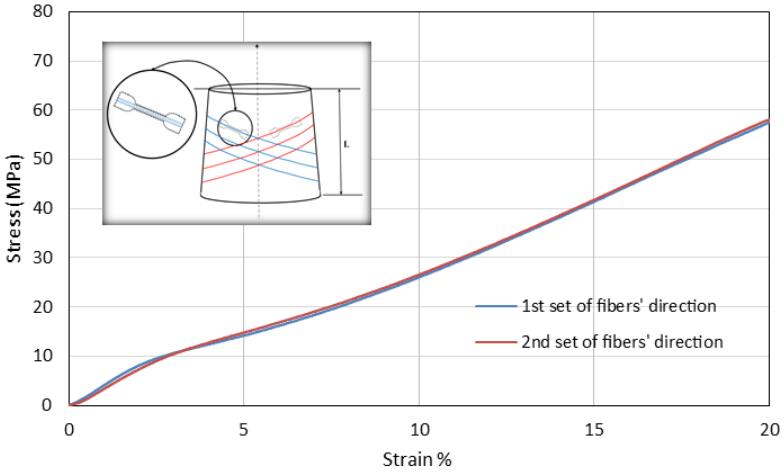

Figure (4): The mechanical behavior of the fiber-reinforced rubber composites tested at a quasi-static speed.

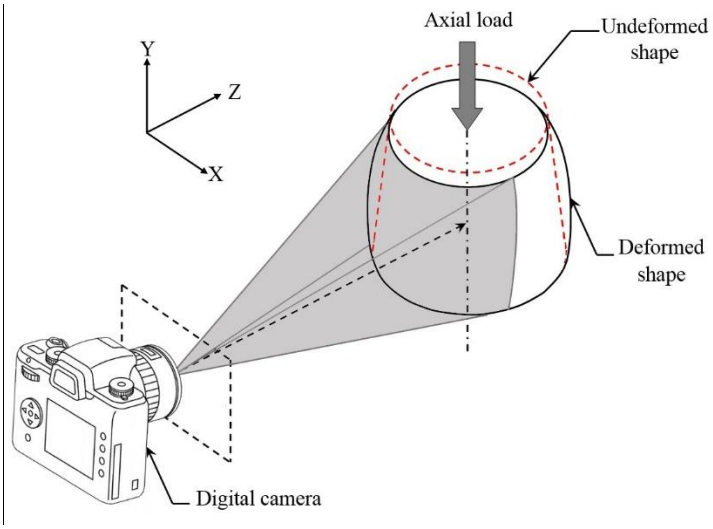

Figure (5): Schematic for the experimental rig.

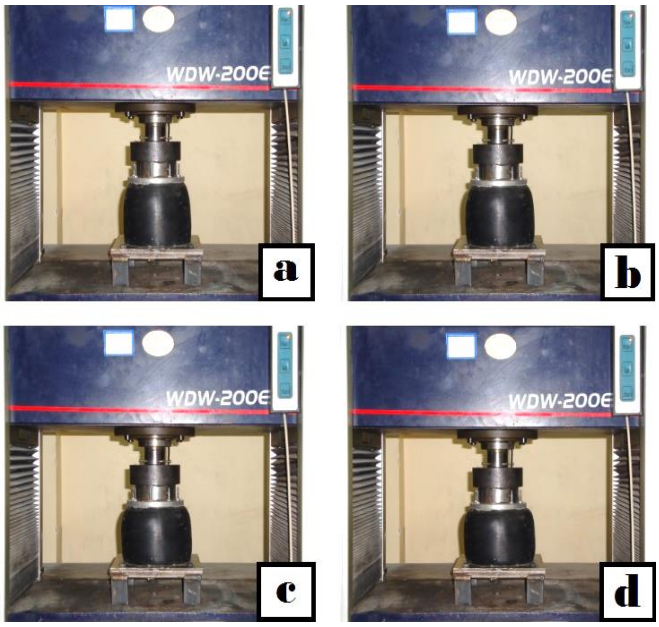

Figure (6): Loading stages of the inflated air-spring pressurized with 0.1 MPa, (a) at free height, (b) displaced 5 mm, (c) displaced 10 mm, (d) displaced 15 mm.

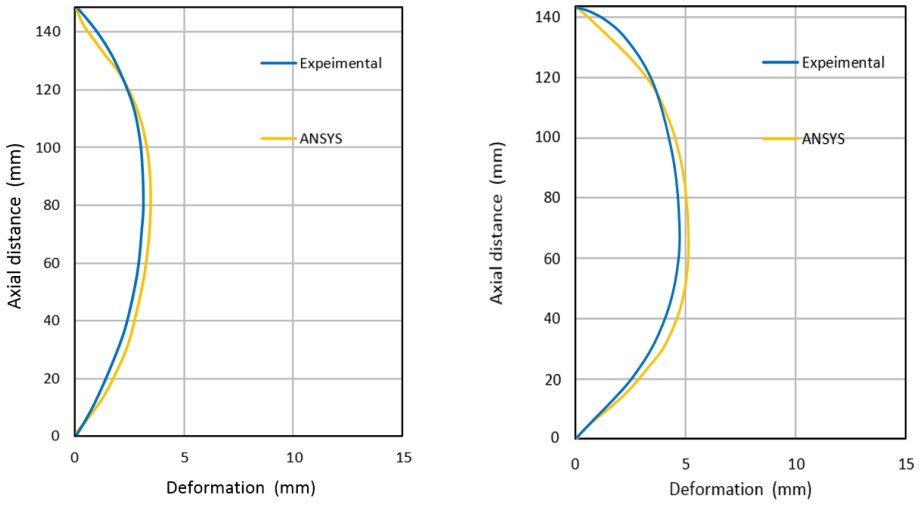

a *b*

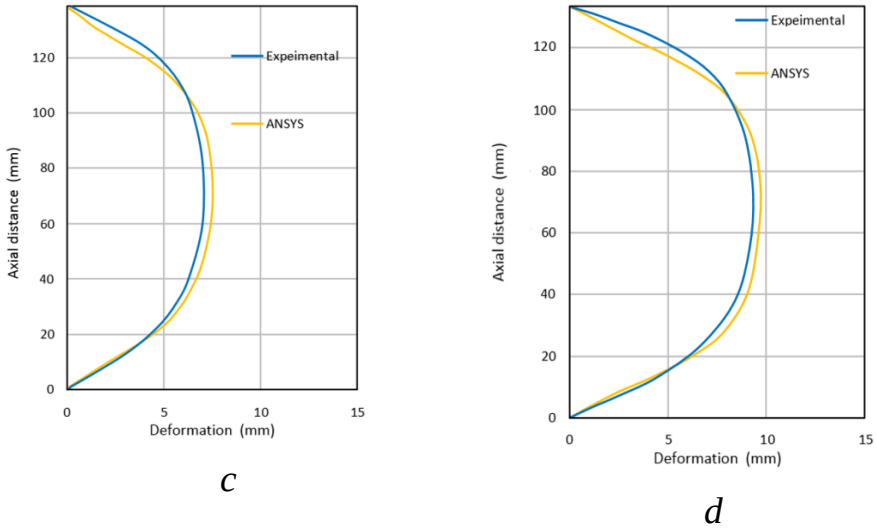

c *d*

Figure (7): A comparison between the experimental and the predicted deformations of the flexible member of the air-spring pressurized with 0.1 MPa, (*a*) at free height, (*b*) displaced 5 mm, (*c*) displaced 10 mm, (*d*) displaced 15 mm.

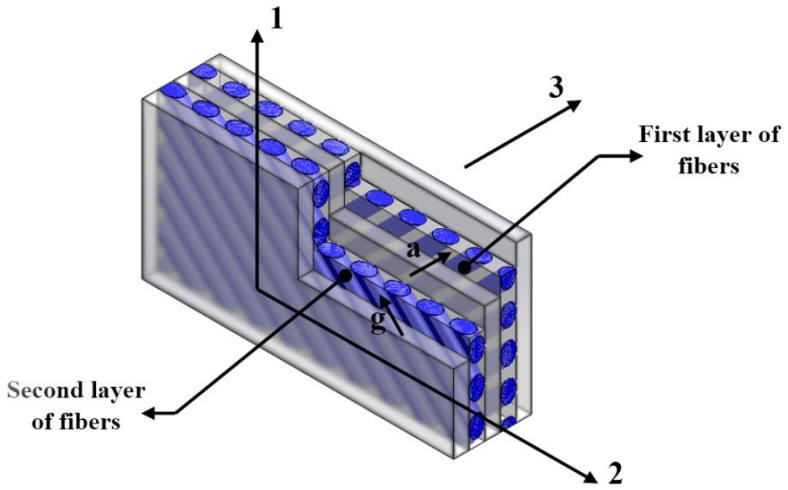

Figure (8): The fibers' orientation inside the rubber.

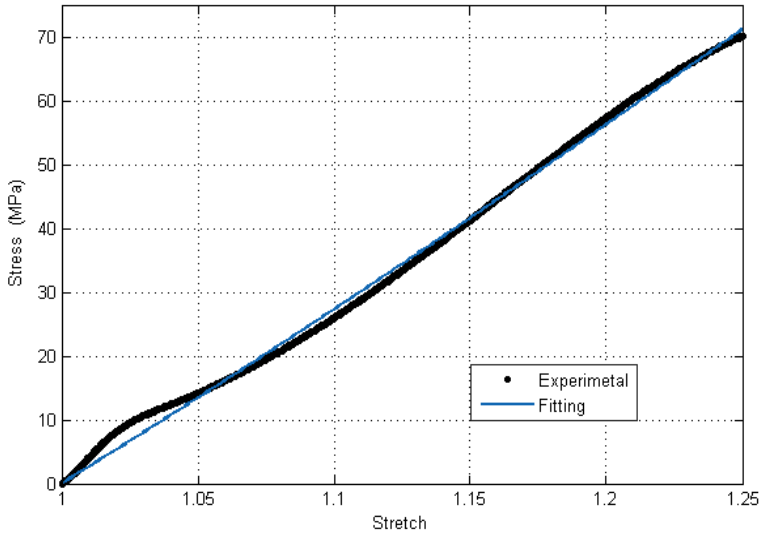

Figure (9): Curve fitting procedure.